7

Spatial Snow Cover Processes at Kühtai and Reynolds Creek

David Tarboton, Günter Blöschl, Keith Cooley,
Robert Kirnbauer and Charlie Luce

7.1 INTRODUCTION

In many climates, predicting and understanding the spatio-temporal variability of snow-related quantities plays a key role in catchment hydrology. Practical applications include the prediction of snowmelt induced floods and the estimation of water yield from snow-covered catchments for water resources management. The snow cover is also a key link in the climate system via its effect on the surface energy and water balance, so its accurate representation is essential to a better understanding of climate effects on the hydrological cycle. Modelling the spatio-temporal variability of snow-related quantities is complicated by the interrelated and multiscale nature of the processes involved. Natural snow variability is extreme and although snow related data such as snow water equivalent is often available in considerable temporal detail as time series (e.g. the US SNOTEL network, NRCS, 1998), the spatial resolution of snow-related data is notoriously poor. Often, at best, a few point measurements are available in the catchment of interest and, because of the extreme spatial variability, point data are not very representative of the spatial patterns and/or the spatial averages. Although runoff does provide a spatially aggregated estimate of melt water yield from a catchment, it is not possible to infer the actual melt processes and their spatial distribution from runoff data alone. Recently, progress in remote sensing of snow has shown potential. Snow-covered area can be measured using a variety of methods. However, remote sensing of snow water equivalent has not been sufficiently developed for operational observation of deep snowcover in rugged mountain terrain (Elder et al., 1998). Therefore it has been suggested in the literature (e.g., Blöschl et al., 1991b) to use snow cover patterns for evaluating and improving distributed snow models. This is consistent with the general thrust of this book of using observed patterns for assessing distributed models. As compared to other components of the hydrologic cycle described in this book such as rainfall, runoff and soil moisture, snow has the definite advantage that

Rodger Grayson and Günter Blöschl, eds. *Spatial Patterns in Catchment Hydrology: Observations and Modelling*

the patterns are actually visible to the eye. However, snow cover related fluxes, state variables and model parameters are highly variable in space and time.

This chapter addresses the issues of spatial variability in snow cover and snow water equivalent, and the processes responsible for this variability. The chapter starts with a brief description of the physical processes involved in snow accumulation, redistribution and melting with an emphasis on their spatial variability. A few key modelling approaches are summarised. Two case studies in different snow environments are discussed to exemplify the range of snow processes typically encountered in catchment hydrology. The first case study is set in the Austrian Alps and is representative of the high alpine environment where snow redistribution by avalanching and differential melting caused by terrain aspect are major sources of spatial variability. The second case study is set in the Western U.S. rangelands where slopes tend to be flatter and wind drift is a major source of spatial snow variability. We conclude with a few remarks on the future of distributed snow modelling and use of spatial patterns to improve model confidence.

7.2 SPATIAL VARIABILITY OF SNOW-RELATED PROCESSES

7.2.1 Snow Accumulation and Melt at the Point Scale

Snow accumulation and melt is spatially variable due to the spatial variability in the driving processes and inputs. This spatial variability in turn results in spatially variable surface water inputs from snowmelt that affects runoff and soil moisture discussed in other chapters of this book. The spatial variability of snow-related processes has been discussed in detail by Obled and Harder (1979) and Hardy et al. (1999), and others. Here we will only give a brief review.

At a point, the accumulation and ablation of snow is a process involving fluxes of energy and mass across the snow–air and the snow–ground interfaces. Energy exchanges include shortwave solar radiation (direct solar radiation and diffuse solar radiation), terrestrial/atmospheric longwave radiation, turbulent fluxes (sensible and latent heat exchanges between the atmosphere and snow), energy fluxes associated with exchanges of mass (the energy that comes with falling rain and is carried away by meltwater), and conduction between the snow and underlying ground (i.e. ground heat flux). In alpine environments, radiation fluxes are usually larger than sensible and latent heat fluxes, but in lowlands where snowmelt tends to occur in early winter they can be much smaller (e.g., Male and Gray, 1981; Braun, 1985). Advective exchanges and the ground heat flux are usually very small, but their integrated effect over a season can be significant. Mass exchanges consist of precipitation inputs, meltwater release, and condensation/evaporation/sublimation, the latter being very small. The dynamics within a snowpack are quite complicated, involving energy and mass fluxes due to conduction, thermal radiation, vapour diffusion, meltwater movement, settling and compaction. Some of these processes lead to the formation of ice layers,

which impede the downward propagation of infiltrating meltwater, resulting in concentrated finger flow and sometimes lateral flow (Colbeck, 1978, 1991).

7.2.2 Spatial Patterns of Snowmelt Processes

Energy exchanges are the main processes responsible for the differential melting of snow in a catchment. The spatial variability of direct solar radiation within a catchment is dominated by terrain slope, aspect and shading. Direct solar radiation per unit horizontal area averaged over a time interval from t to $t + \Delta t$ may be expressed as

$$Q_{si} = I_o \cdot T_f \cdot \frac{1}{\Delta t \cos S} \int_t^{t+\Delta t} \cos(\psi(t))\mathrm{d}t \tag{7.1}$$

where I_o is the solar intensity (4914 kJ m^{-2} hr^{-1} or 1367 W/m^2), T_f atmospheric transmissivity, S the local slope angle and $\psi(t)$ the time varying illumination angle, defined as the angle between the surface normal and direction to the sun. In mountain regions, terrain shading can be important in which case the integral above should only be evaluated for times when direct radiation is incident, i.e. the point is not shaded by nearby terrain. The time varying illumination angle can be accurately computed from analytical expressions and tabulated values (Dozier, 1979). Atmospheric transmissivity depends upon weather conditions and cloudiness and therefore gives rise to the largest uncertainties in estimation of incident radiation. Simple approaches to quantifying atmospheric transmissivity include those of Bristow and Campbell (1984) based upon diurnal temperature ranges and Neuwirth (1982) based on visual observations of cloudiness (i.e. the fraction cloud cover of the sky). More elaborate methods integrate radiative transfer throughout the atmosphere (e.g. "LOWTRAN 7", see Kneizys et al., 1988). The spatial distribution of atmospheric transmissivity in a catchment is random and hence essentially unpredictable but fortunately, if integrated over a period of say a few weeks, its effect on snowmelt tends to average out, so approximating transmissivity as constant over a study area is usually reasonable.

Part of the atmospheric transmissivity reduction in direct radiation is due to scattering and about one half of the scattered energy reaches the surface as diffuse radiation (the other half going out into space) (Dingman, 1994). Diffuse radiation tends to increase in cloudy conditions when more of the incident radiation is scattered. In a catchment, the spatial pattern of diffuse radiation received by the snow surface depends on the fraction of the sky dome that is visible from each point. This fraction can be quantified in terms of the sky view factor, V_d. The sky view factor is based on the assumption of isotropic radiation and is defined as the ratio of the radiation incident on a point accounting for slope, aspect and terrain obstructions, to the equivalent radiation incident on a flat and unobstructed surface. V_d only depends on terrain and does not depend on time. For any point in time, incident diffuse shortwave radiation can be estimated as

$$R_{\text{slope}} = V_d \cdot \pi \cdot I_d \tag{7.2}$$

where I_d is the isotropic diffuse radiation intensity. In mountain regions, solar radiation reflected by surrounding terrain can also be important. It can be approximated by $(1 - V_d)$ times reflected shortwave radiation (albedo times incident radiation). Procedures for computation of horizon angles and sky and terrain view factors and discussion of their use, assumptions and limitations in estimating radiation are given by (Dozier, 1979; Dozier and Frew, 1990; Dubayah et al., 1990; Frew, 1990).

Part of the incoming solar radiation is reflected by the snow surface. The ratio of reflected and incoming radiation is termed albedo, which can vary considerably as a function of the condition and age of the snow surface. Given the magnitude of the solar radiation term in the energy balance, modest albedo changes are important to the snow surface energy balance. The albedo of snow is generally at a maximum after a fresh snowfall and decreases with time due to growth in grain sizes, and the accumulation of dust, soot and debris on the snow surface (U.S. Army Corps of Engineers, 1956). The rate of grain growth increases with snow temperature and in particular with the presence of liquid water (Wiscombe and Warren, 1981; Dozier, 1987; Marshall and Warren, 1987). The most important process controls on albedo are reflected in the parameterisations suggested by various authors. Examples include Rohrer (1992) and Dickinson et al. (1993) who proposed a parameterisation of albedo as a function of air temperature and time after snowfall, Brun et al. (1992) who parameterised albedo as a function of time after snowfall, grain size and grain type, and Marks and Dozier (1992) and Marshall and Warren (1987) who modelled grain size increase and parameterised albedo in visible and infrared bands as a function of grain size. Little is known about the spatial distribution of snow albedo in catchments; the controls mentioned above do suggest that albedo tends to be lower on south-facing slopes (in the Northern Hemisphere) due to the more rapid grain growth as a consequence of larger energy inputs as compared to other slope aspects.

Both the atmosphere and the snow surface emit black body longwave radiation that is proportional to the fourth power of absolute temperature. Incoming longwave radiation from the atmosphere is related to the vertical distribution of air mass properties (air temperature, vapour pressure) and the presence of clouds (Obled and Harder, 1979). While several parameterisations are available based on surface air temperature and vapour pressure (see e.g., Price and Dunne, 1976; Satterlund, 1979) there is considerable uncertainty in these estimates due to atmospheric variability. Radiative transfer models (e.g. "LOWTRAN 7", see Kneizys et al., 1988) overcome some of this uncertainty at the cost of more substantial data requirements. In a valley, incoming longwave radiation from the atmosphere is reduced because the adjacent mountains obscure part of the sky. Like shortwave diffuse radiation, incoming longwave radiation from the atmosphere is generally diffuse and its spatial pattern can be represented by the sky view factor analogously to equation (7.2). However,

scattered and emitted longwave radiation from mountainside slopes is present and may be greater than atmospheric longwave radiation, particularly in steep valleys and cirques where the slopes are snow free. For example, Olyphant (1986) showed that the snowpack in cirques can have an additional longwave radiation input from the surrounding terrain equivalent to 500 mm melt when integrated over an entire snowmelt season, as compared to flat terrain. Similar to reflected shortwave radiation, it can be approximated by $(1 - V_d)$ times terrestrial emissions from surrounding terrain.

Outgoing longwave radiation is on average greater than incoming longwave radiation, resulting in a net loss of energy as thermal radiation from the surface. The emissivity of snow is between 0.97 and 1 (Anderson, 1976) and night time longwave radiation losses under clear skies are responsible for considerable cooling of the snow surface. However, actual heat loss is limited by the small thermal conductivity of the snow which may vary depending on snow surface properties. The spatial distribution of longwave radiation emitted by the snow in a catchment is rather complex, being controlled by the spatial pattern of surface temperature, which in turn is controlled by the overall heat budget of the snow. Cold snowpacks (prior to any melting) have low thermal conductivity which results in limited outgoing longwave radiation and large night-time depressions in surface temperature. The presence of liquid water in the snow near the surface, due to melting or rain, alters this significantly. The surface temperature remains close to freezing (0 °C) until this water refreezes. This unfrozen water near the surface represents a considerable storage of latent heat of fusion energy that may be radiated away. Melting and refreezing also results in crusts at the snow surface with altered thermal properties (conductivity and density). These processes are the compound effect of total net energy exchanges and vary spatially because of the terrain effects on incident radiation energy inputs.

Incident radiation (both shortwave and longwave) on snow beneath the vegetation canopy is limited by the radiative transmissivity of the vegetation (Verstraete, 1987, 1988; Verstraete et al., 1990) which is related to leaf area index defined as the ratio of the total surface of leaves above a ground area to that ground area, as well as leaf shape and orientation. Vegetation has a lower albedo than snow, and therefore absorbs more incident radiation and may be warmer than the surrounding snow surface. Vegetation emits longwave radiation proportional to the fourth power of its absolute temperature which results in localised melting around sparse vegetation. Vegetation also provides greater surface roughness, reducing wind speeds at the surface of snow beneath vegetation which affects the turbulent energy transfers mentioned below. In sparsely vegetated areas, the persistence of snow patches associated with patches of vegetation is a source of spatial variability, due to vegetation shading as well as wind sheltering and accumulation of snow drifts (Seyfried and Wilcox, 1995). The spatial pattern of vegetation is naturally quite variable due to temperature, radiation and moisture variability and the biological needs of different species and in most environments it is controlled by human activity which adds additional variability. This spatial variability influences the distribution of snow, and is

influenced by snow distribution in a synergistic relationship. Snowmelt supplies water for vegetation. Snow also affects the environment in which vegetation species need to survive.

Turbulent energy transfers comprising sensible and latent heat fluxes are a significant component of the snow energy balance. Sensible heat fluxes depend on the temperature gradient and turbulent diffusion due to wind. Latent heat fluxes depend on the vapour pressure gradient and turbulent diffusion due to wind. Latent heat fluxes consist of evaporation and condensation of liquid water, and sublimation of ice (Male and Gray, 1981; Bras, 1990). Surface roughness and the profile of wind velocity with height control turbulent diffusion. Turbulent transfer rates also depend on atmospheric stability, which is a function of the temperature gradients (Brutsaert, 1982). Snow surfaces with surface temperature limited to remain at or below melting (0 °C) almost always have a stabilising effect on the atmosphere, tending to reduce turbulent diffusion. Spatial variability of topography and vegetation result in spatial variability in wind, wind profiles and turbulent energy fluxes which affect the spatial patterns of snow. Windspeed is higher on exposed ridgetops than in valleys. Windspeed is also higher on upwind than on downwind slopes. The variability of wind will be discussed below in the context of wind redistribution of snow where it has a greater effect. The same wind spatial variability that results in snow redistribution also has spatially variable effects on turbulent exchange.

7.2.3 Spatial Patterns of Snow Accumulation Processes

Snowfall and snow redistribution by wind are the main processes responsible for the differential accumulation of snow in a catchment.

The main control on snowfall patterns is elevation through its control on the state of precipitation. The state of precipitation (rain or snow) depends upon air temperature at the time of precipitation. The lapse rate of air temperature with elevation results in snow at higher elevations and rain at lower elevations. The snow line (the elevation separating rain from snow) varies for each precipitation event. Rain on snow may cause snowmelt at lower elevations, while at high elevation there is additional snow accumulation. The net effect of these processes is a strong dependence of snow accumulation on elevation. In addition to the effects due to the state of precipitation discussed above, topography also influences the pattern of snowfall and accumulation through orographic effects on atmospheric processes. Heavy precipitation occurs on slopes where atmospheric flow is forced over mountain ranges. Orographic lifting may also induce instability in the atmosphere, triggering convective precipitation (e.g., Dingman, 1994). On the downwind side of mountain ranges, precipitation is reduced because orographic lifting and condensation have stripped moisture from the atmosphere. Approaches to modelling orographic precipitation range from empirical correlation of precipitation with elevation, the so-called hypsometric method (e.g., Dingman, 1994; also see Chapter 2, pp. 35, 40), to

models that empirically and dynamically model atmospheric flow and snowfall (Rhea, 1978; Peck and Schaake, 1990; Barros and Lettenmaier, 1993, 1994). The scale of spatial patterns associated with orographic effects is generally quite large (1 km or more) relative to the variability associated with, for example, slope and aspect effects on radiation (10 to 100 m).

In steep terrain, deposited snow frequently sloughs and avalanches, moving downslope under the influence of gravity in sometimes catastrophic fashion, coming to rest in less steep gullies and runout zones. The two main controls on sloughing and avalanching are terrain slope and the stability of the pack. Typically, hillslopes with slopes between 20° and 50° are prone to avalanching while steeper and flatter slopes are not. Avalanches usually originate in weak layers resulting from variable snow density, crystalline structure and lack of bonding between new and old snow (e.g. McClung and Schaerer, 1993; Armstrong and Williams, 1986). On flatter slopes the downslope component of gravity is insufficient to overcome the shear strength of snow.

The redistribution of snow by wind is a complex process controlled by the interaction of wind flow, topography, snow properties and surface roughness. Processes involved include scour from upwind slopes, sublimation of suspended and saltating particles, deposition on downwind slopes and especially behind terrain obstacles, where flow separation occurs. Vegetation, through its influence on surface roughness, limits the scour and enhances the deposition of blowing snow. This effect of vegetation is only present while it is not buried by snow, leading to the concept of vegetation holding capacity used in wind-blown snow modelling (e.g., Pomeroy and Gray, 1995; Liston and Sturm, 1998).

This section has shown, in a conceptual fashion, the physical processes that lead to spatial variability and spatial patterns in snow accumulation and melt. These comprise multiple processes interacting across a range of scales. McKay and Gray (1981) summarise the scales involved in various snow redistribution processes:

- Macroscale: (10^4–10^5 m) Elevation, orography, meteorological effects such as standing waves, flow of wind around barriers and lake effects.
- Mesoscale: (10^2–10^3 m) Redistribution due to wind and avalanches, deposition and accumulation related to elevation, slope, aspect, vegetative cover height and density.
- Microscale: (10–10^2 m) Primarily surface roughness and transport phenomena.

In the next section we review approaches for distributed snow modelling followed by case studies where spatial patterns of distributed measurements and model results are compared.

7.3 SPATIAL SNOW MODELLING

Spatially distributed snow models differ in terms of the degree of process representation they involve. At one end of the spectrum are empirical methods that

often use statistical relationships involving temperature, radiation and terrain properties while at the other end are process based (dynamic) models (Kirnbauer et al., 1994). One example of an empirical model for estimating peak snow accumulation is the SWETREE model (Elder, 1995; Elder et al., 1995, 1998; Winstral et al., 1999). This model is based on statistical analysis of a very large number of snow water equivalent samples and uses binary decision trees to predict snow water equivalent based upon indices for radiation, wind exposure and other controls. These indices are used to subdivide a catchment into classes, starting from the most important controls and proceeding to the less important controls. A similar recent example is the model of König and Sturm (1998) which is based on topographic rules using physiographic features such as creek patterns, flat patterns, and slope patterns. These features are derived from a visual analysis of aerial photographs, and for each of them, characteristic values of snow depth and snow water equivalent are assigned. König and Sturm (1998) examined their method in the Alaskan Arctic where slopes are much flatter than in the catchments of Elder (1995) and where wind drift is the main process giving rise to differential accumulation and melting. Another contribution to mapping snow water equivalent is due to Woo et al. (1983) and Yang and Woo (1999) which, similar to König and Sturm (1998), use topographic features, but their approach is more heavily based on ground data. The advantage of this type of model is a parsimonious model structure which implies robustness and ease of use, but this comes at the cost of requiring a substantial database for calibrating the model, usually consisting of both remotely sensed images and ground data. An example of an empirical spatially distributed melt model is provided by Williams and Tarboton (1999). This model separates the energy that causes snowmelt into three components: a spatially uniform component, a component that is proportional to elevation, and one that is proportional to solar illumination (which is determined from topography). Measurements of snowmelt at several topographically unique points (called ''index points'') in a catchment are related to elevation and solar illumination through regression in order to factor the melt energy into the three separate components at each time step. Inputs from snowmelt measurements at the index locations are used to calibrate the regression at each time step. Then the spatial patterns of solar illumination and elevation are used to predict the spatial distribution of melt over the whole catchment.

Process-based models account for both mass and energy exchanges and keep track of state variables related to mass and energy over time. In this type of model, the catchment is usually subdivided into model elements and point snow models are applied to each element. There have been a large number of point snow models developed in the literature that range in complexity and amount of data used (e.g., Anderson, 1976; Blöschl and Kirnbauer, 1991; Jordan, 1991; Kustas et al., 1994; Tarboton et al., 1995; Tarboton and Luce, 1996; Luce et al., 1997). The main advantage of this type of model is that it allows a detailed representation of the processes giving rise to differential melting and accumulation. However, extension of point snowmelt models to catchments involves considerable problems and uncertainty, part of which is related to scale issues (e.g.

Kirnbauer et al., 1994; Beven, 1995; Blöschl, 1999). As discussed in a general sense in Chapter 3, the fundamental questions involve the selection of model elements, parameterisation of subgrid variability and nonlinearity, and distributing input data and model parameters across the catchment. Ways of selecting model elements in distributed snow models are similar to those in other hydrological models and include square grids, hillslope elements, and elevation bands (see Chapter 3).

If these elements are small enough, a detailed spatially explicit approach is possible. While this approach is conceptually simple and appealing, we must have enough detailed information to determine site parameters and inputs to each element. However, this is often not possible and element sizes are used that are relatively large as compared to the characteristic scale of the underlying variability. Often, the effective parameter approach is used where it is implicitly assumed that an average parameter over that element represents the combined effects of the processes within that element (see Chapter 3, p. 00) but as snow related processes are highly nonlinear, treatment of the variability within elements (i.e. subgrid variability) requires particular attention. Luce et al. (1997), for example, showed that this approach may yield incorrect results once the element area exceeds about 1 ha. An alternative is to use distribution functions to represent subgrid variability. The distribution function approach so far has not been widely used for representing subgrid variability in spatially distributed snow models but it has a long tradition for representing spatial variability in lumped catchment models. An early example is the areal depletion curve approach of Anderson (1973), where an empirical function is used to relate the areal extent of snow cover to mean areal water equivalent. A more recent example is Luce et al. (1999) who show that the surface water input estimated from a lumped model parameterised with a depletion curve derived from the distribution of snow at peak accumulation, compares well with the surface water input estimated from periodic measurements and from an explicitly distributed snowmelt model. A drawback of using spatial distribution functions within each model element is that one needs a minimum of two or three parameters to represent the distribution functions rather than one single parameter as in the effective parameter approach, but it is much better suited for representing the nonlinear effects of the subgrid snow processes.

Distributing input data and model parameters across the catchment draws on the understanding of the spatial variability of the processes driving snowmelt and snow accumulation. Climatic data are usually available at one or two sites within the catchment and snow courses usually provide just a few values of snow water equivalent and snow depth, so distributing this information to every model element requires assumptions to be made. This distribution procedure is essentially an interpolation problem, i.e. a problem of determining patterns from points (see Chapter 2). In the context of snow, auxiliary data for interpolation can be based on terrain features such as slope, aspect, terrain shading and view factors that can be directly computed from digital elevation models. As discussed earlier in this chapter, this approach is particularly useful for estimating detailed spatial pat-

terns of radiation inputs to snowmelt models (Dozier, 1979; Dozier and Frew, 1990).

One of the most important issues of spatial snow models is how to represent snow redistribution by wind drift. There are three types of approaches in the literature that differ in complexity. The simplest approach is to use wind drift factors. The basic assumption of this approach is that the spatial patterns of snow and/or snowfall are similar in all years. This similarity is based on the rationale that topography is the main factor controlling wind drift and that average wind speeds and directions only differ slightly from year to year. It assumes that if snowfall is increased, the amount of accumulated snow water equivalent will be increased proportionally and the spatial pattern due to drifting will be the same. In an alpine environment, Kirnbauer and Blöschl (1994) found that this is indeed the case, with acceptable accuracy. Once the time stability is established, there are two possibilities of deriving the wind drift factors. The most accurate approach is to sample snow water equivalent exhaustively in the catchment (e.g. Cooley, 1988) and to derive snow drift factors from these data (Tarboton et al., 1995; Luce et al., 1998). For larger catchments this is not feasible, and relationships between wind drift factors and topographic attributes have been postulated (e.g. Blöschl et al., 1991b; see discussion in Moore et al., 1996). The parameters for these types of relationships can be estimated from remote sensing data and/or ground measurements. A further step up in complexity is quasi-dynamic models. A typical representative of this model genre is given in Essery et al. (1999). They applied a model of wind flow over complex terrain to arctic landscapes and used it to investigate joint probability distributions of wind speed and blowing snow occurrence. Functions that describe the joint distribution were then used to scale results up from a single-column model of blowing snow that presumes homogeneous terrain. Results are compared with results from a distributed model and spatially distributed snow surveys from the Arctic. The most complex models are dynamic models. One example is the model of Liston and Sturm (1998) which represents snow transport resulting from saltation and suspension, snow accumulation and erosion, and sublimation of the blowing and drifting snow. It is driven by a wind model that computes the flow field over the complex topography. Model inputs include climatic forcings, as well as vegetation type which is used to determine a vegetation snow-holding capacity that must be exceeded before any additional snow is available to be transported by the wind. The complex air flow in an alpine environment provides a challenge for these models, therefore in many cases one must resort to the more empirical model types for representing snow redistribution by wind drift.

In the following sections we will present two case studies. The aim of the case studies is to deterministically model spatially distributed snow processes in small catchments. The case studies differ greatly in terms of their hydrological and climatological settings, and in terms of the processes giving rise to spatial snow variations. The Kühtai study is set in steep alpine terrain with high annual precipitation, deep snowpacks and an extended ablation period. The Reynolds Creek study is set in undulating rangelands where precipitation is low and most

of the snowmelt occurs during a relatively short period. Radiation along with sloughing, avalanching and wind redistribution are important at Kühtai, while wind drift is the most important factor causing spatial snow variations at Reynolds Creek. The catchments also differ in scale, the catchment of the Kühtai study (9.4 km^2) being about 40 times the size of the Reynolds Creek study catchment (0.26 km^2). Climate, terrain and scale have implications for the type of data of snow variability used in the two studies. In the case of Kühtai, remotely sensed snow cover patterns are used (binary values of snow/no snow at about 15,000 pixels) while in the case of Reynolds Creek ground data of snow water equivalent (sampled on a regular grid of about 300 points) are used.

7.4 KÜHTAI CASE STUDY

The Längental catchment is located in the Kühtai region, Tyrol, in the Austrian Alps. The catchment is 9.4 km^2 in size and elevations range from 1900 to 3050 m above sea level. Geomorphologically, the basin consists of two major units (Figure 7.1). The lower part comprises east and west facing slopes including talus fans with typical slopes of 35 to 40°. The upper part in the south west is open to the east. The south-east edge of the basin is formed by three prominent cirques. Most of the catchment lies above the timber line and there are only a few scattered larches and cembra-pines. The flat areas are covered by alpine meadows and the steep areas are rock and debris. Average annual precipitation is about 1200 mm, 50 % of which falls as snow. Temperatures average 10 °C in summer and −5 °C in winter (Figure 7.2, dotted line). In the lower parts of the catchment the snow cover period typically lasts from November to May, reaching maximum snow depths of about 1.5 m in April. The upper parts of the basin are bare only for a few weeks in August or September and maximum annual snow depths are on the order of 4 m. Snowmelt occurs in several episodes during the period from March to late June. Redistribution caused by wind drift, avalanching and sloughing substantially affects the spatial distribution of snow.

In the mid 1980s the Kühtai snow monitoring station was established next to the catchment outlet and was the place of detailed snow hydrological studies (Kirnbauer and Blöschl, 1990). When we considered extending the point-scale studies to the entire Längental catchment, we soon realised that the key to successfully representing the spatial patterns of snow processes would be to get data on the spatial variability of snow depth. There were a number of problems specific to the Längental catchment not usually encountered in research catchments. First, the catchment is inaccessible for weeks at a time due to avalanche hazard. Some of the steep slopes and cliffs sometimes do have snow accumulation but are time consuming to access. Also, the size of 9.4 km^2 with the given logistic constraints made exhaustive sampling of snow depth not an option. We considered a number of possibilities to work around these problems. The first idea was to place a large number of snow stakes in the catchment during the

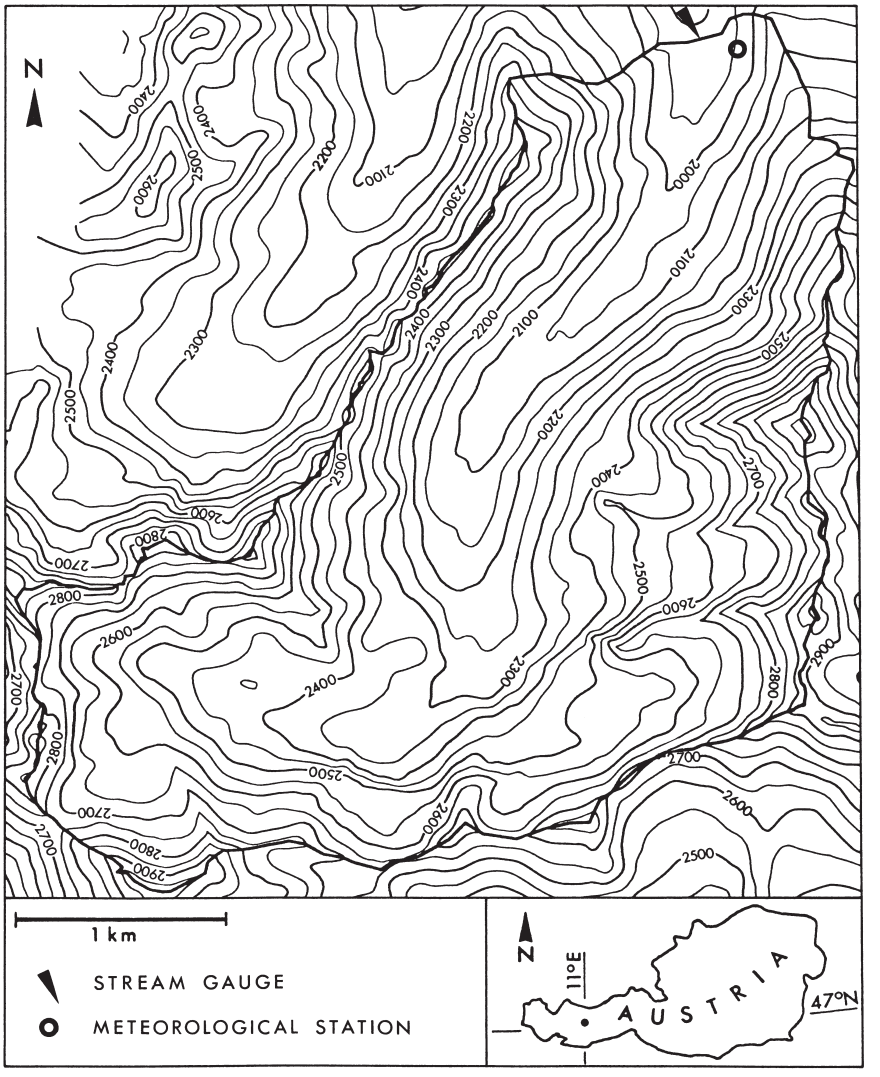

Figure 7.1. Längental basin map. (From Blöschl et al., 1991b; reproduced with permission.)

summer and read snow depth using binoculars. We were hoping to get snow depth to an accuracy of 0.2 m at 100 locations within the catchment. However, it soon became clear that this was not a feasible option because of the rocky subsurface, snow creep and potential problems with conservationists. As an alternative we considered using aerial stereo photographs to estimate the elevation of the snow surface and then calculating snow depth by taking the difference between snow and terrain elevations. With the scale of the photos envisaged we were hoping to get snow depth to an accuracy of 0.5 m exhaustively in the catchment. However, initial tests showed that there is not enough visual contrast on the snow surface for accurate stereo photo interpretation and we therefore abandoned this option. Finally, we decided to use the spatial patterns of snow cover only. Nine aerial surveys were undertaken during the 1989 ablation period,

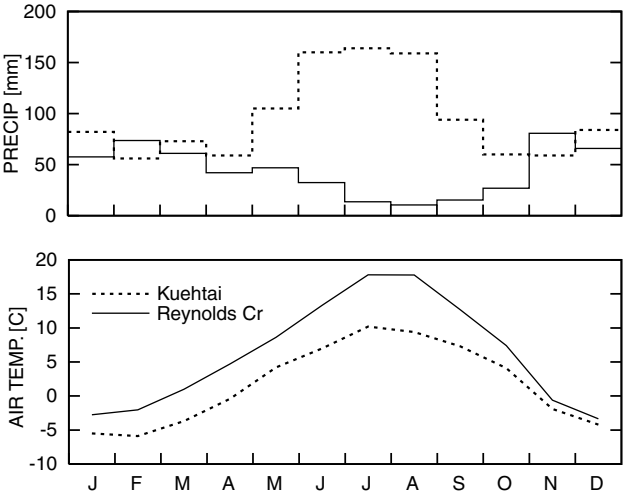

Figure 7.2. Mean monthly precipitation and air temperature at Kühtai, Längental (dotted line), and at Upper Sheep Creek (solid line). The averages are over 1981–1990 and 1983–1994 respectively.

and oblique visual photos of the catchment were acquired. We marked the snow boundary lines manually on the prints. The snow lines were subsequently digitised as vector data, rectified by digital mono-plotting methods (Hochstöger, 1989), and rasterised. As a first step, a 5×5 m grid was used which was then generalised to a 25×25 m grid based on the majority of snow-covered or snow-free 5×5 m pixels in any one 25×25 m pixel (Blöschl and Kirnbauer, 1992). Each pixel value therefore represents the average over the pixel area rather than a grid point value. Although this methodology provided only binary information of snow-covered and snow-free pixels, comparisons indicated that this information was extremely accurate. We chose to have a large number of points with simple information (i.e. binary values from photo interpretation) rather than fewer points with detailed information such as is possible with snow courses (see discussion on the trade-off between accuracy and spatial detail in Chapter 2, pp. 24–5).

However, we did also get some snow course data to complement the aerial survey. A field program was undertaken in late April to assess the distribution of water equivalent in the basin. As we could only sample a small number of sites, the selection of sites was based on typical terrain types as outlined by Woo et al. (1983) and Yang and Woo (1999). These sites included different elevations, slopes and aspects. Measurements were designed to be representative of an area of roughly 50×50 m each, accomplished by numerous snow-depth measurements over that area and a few density profiles.

A snowmelt model (the Vienna University of Technology Snow – VUTS model) was set up for the Längental catchment based on a 25 m grid. For each grid element the energy balance components were simulated and the coupled heat and mass flow within the snowpack was simulated by a multilayer model (Blöschl and Kirnbauer, 1991). Atmospheric data used to drive the model included incoming shortwave radiation, air temperature, humidity, wind speed

and precipitation on an hourly basis. These variables were observed at the Kühtai station (1930 m elevation) near the basin outlet. Cloudiness was determined from visual observations. Additional air temperatures at Finstertal (2330 m elevation, 700 m east of the catchment boundary) were also used. Inputs of air temperature were assumed to decrease linearly with elevation based on the readings at the two stations. Wind speed and relative humidity were taken as invariant across the catchment. Horizon shading, and aspect and slope dependence of solar radiation input were accounted for by using equation (7.1). One of the essential assumptions was that terrain attributes could be used to represent the effects of wind drift and sliding as discussed below. Also, as we were running the VUTS model only for the ablation period, initial conditions for the spatial distribution of snow water equivalent within the catchment had to be stated. For both snowfall and initial snow water equivalent we postulated a wind drift factor F of the form

$$F = (a + b \cdot H) \cdot (1 - f(S)) \cdot (1 + e \cdot C) \qquad \geq 0 \tag{7.3a}$$

$$f(S) = \begin{cases} 0 & \ldots \quad S < c \\ \dfrac{S - c}{d - c} & \ldots \quad \text{otherwise} \end{cases} \tag{7.3b}$$

where H is elevation, S is slope and C is terrain curvature at the grid scale of the digital elevation model. For the case of solid precipitation a and b were chosen so as to give a 30 % increase of precipitation with elevation from the lowest to the highest part of the catchment. For the case of initial snow water equivalent a and b were estimated from snow course data. c, d and e were derived from an interpretation of the aerial photos of the snow cover as $c = 10^\circ$, $d = 60^\circ$, and $e = 50$ m (Blöschl and Kirnbauer, 1991). A discussion of this approach is given in Moore et al. (1996).

Figure 7.3 (top) shows the initial snow cover pattern on April 24, 1989 as used for the model initialisation. The other patterns are observations and simulations for May 22, June 14, and June 26, 1989. There is a good agreement of percent snow-covered area. Observed and simulated snow-covered areas, respectively, are 64 % and 70 % for May 22; 46 % and 46 % for June 14; and 31 % and 33 % for June 26. Observed and simulated snow patterns are, overall, also quite similar but there are some differences. We will use these differences to infer potential misrepresentations of snow cover processes in the model.

The simulations for May 22, 1989 in Figure 7.3 indicate that in the northern part of the catchment near the catchment outlet (particularly in the valley floor) snow cover is slightly overestimated, and the simulated snow cover is spatially more coherent than in the observations. This suggests that the VUTS model also overestimated snow water equivalent in this part of the catchment. Conversely, on June 14, 1989 the model tends to underestimate snow cover (and consequently probably snow water equivalent) in the same part of the catchment, which must be related to too fast a depletion of the snowpack from May 22 to June 14. These inconsistencies are believed to be due to two reasons. (a) There was fair weather with substantial melting from May 22–31, snowfalls in the entire catchment from June 1–9, and again fair weather from June 10–14. While the model does simulate

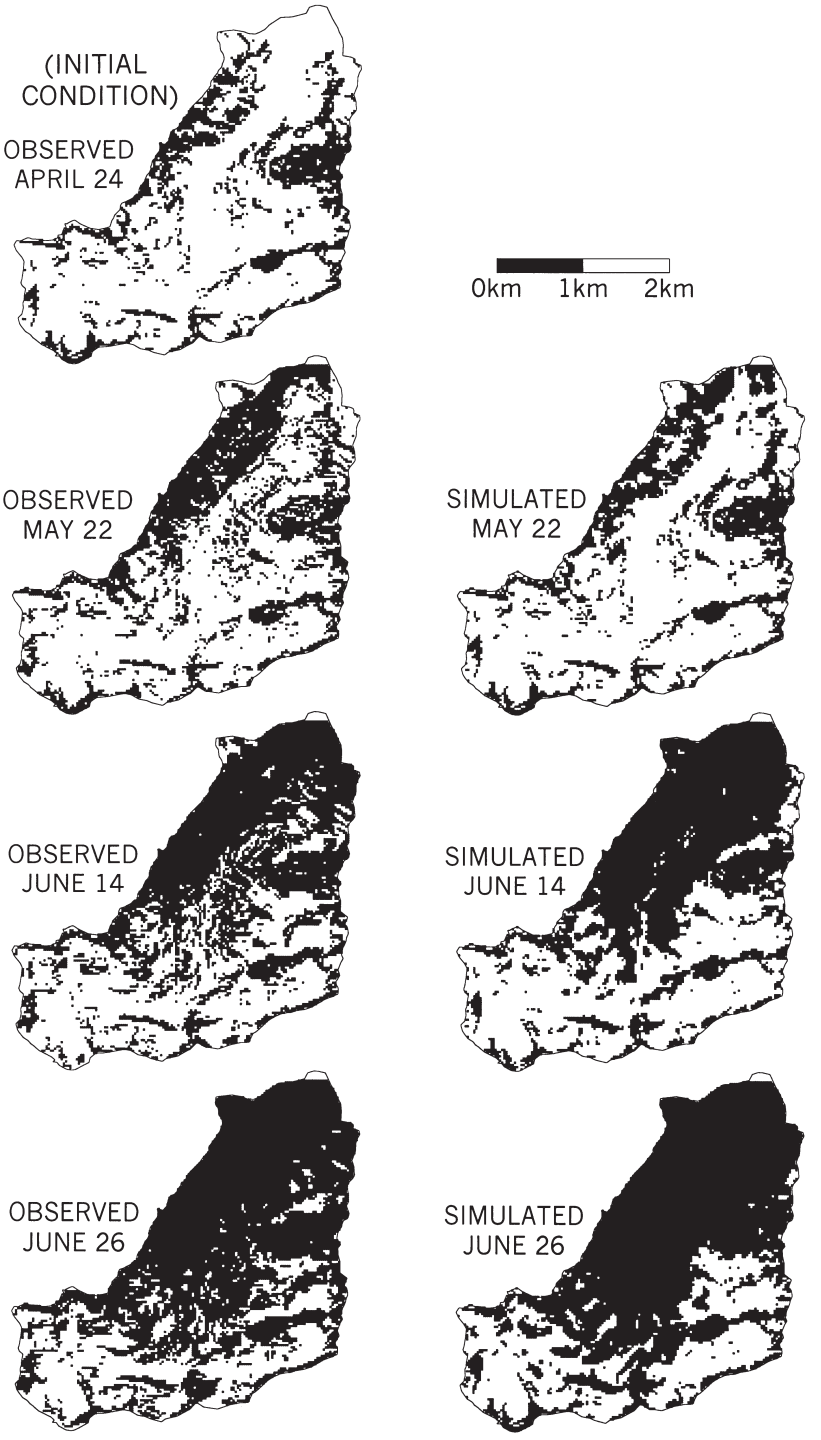

Figure 7.3. Observed and simulated snow cover patterns at Kühtai. Top left: observed snow cover April 24, 1989 (initial condition). Left column below: observed snow cover on May 22, June 14, and June 26, 1989. Right column: model simulations for the same dates. Dark areas denote bare ground and light areas denote snow cover.

albedo as a function of time after snowfall, it is likely that the parameter value for new snow albedo was set too low which caused an overestimation of melt, particularly after the snowfalls. (b) The inconsistencies may also be due partly to the effect of wind blown snow which, on May 22, accumulated in the valley floor more strongly and, on June 14, depleted the north-west facing slopes in the centre of the catchment more rapidly than predicted by equation (7.3). It is important to note that equation (7.3) uses terrain parameters (including curvature) at the grid scale of the terrain model (i.e. 25 m) while the scale of wind drift processes and the scale at which terrain affects wind drift patterns range from smaller to much larger scales than 25 m. One potential remedy would be to use a wind drift factor F that also uses terrain information at larger scales that can be derived from a lower resolution terrain model. This approach has shown potential in another Austrian catchment (Kraus and Blöschl, 1998). The simulations for June 26, 1989 in Figure 7.3 indicate an overprediction of snow cover in the south-eastern part of the basin which is formed by three prominent cirques. The rockwalls of the cirques are bare during most of the ablation period and hence may substantially enhance energy input to the snow cover in the cirque (Olyphant, 1986). We therefore believe that part of this overprediction derives from neglecting longwave radiation emissions from bare surfaces and their interaction with the snow cover.

To better visualise the effects of terrain on model results, the simulated snow pattern for June 26, 1989 in Figure 7.3 was plotted as a perspective view and compared to the oblique photo (Figures 7.4 and 7.5). One apparent inconsistency of observed and simulated snow patterns is an underestimation of snow cover at the base of the steep cliff in the centre of the photo. It is clear that a massive snow deposit had formed there due to sloughing and wind drift from the upslope area. Although equation (7.3) does account for wind drift, it does so in a simplified way and does not explicitly route blown snow and avalanches. Although the average conditions are captured well, situations such as the base of a steep cliff are not represented so well. One potential improvement over equation (7.3) would be a model that deterministically routes snow as a function of terrain and wind conditions.

Another minor discrepancy in Figures 7.4 and 7.5 is that the simulations tend to exhibit fewer small patches of snow. Clearly, they are related to small-scale (subgrid) variability not explicitly accounted for in the model. Although it is not clear how this subgrid variability affects the mean catchment simulations it does highlight the limitations of using point measurements for representing spatial averages of snow water equivalent and snowmelt.

Figure 7.6 shows an evaluation of simulation errors on an element-by-element basis for June 26. The elements are subdivided into classes according to slope and aspect separately for the upper part (> 2400 m, dashed lines) and lower part ($\leqslant 2400$ m, solid lines) of the basin. The labels on the vertical axes relate to the disappearance of the snow cover as simulated by the model. The percentage denoted by "too late" refers to elements with snow cover simulated and bare ground observed, i.e. an overestimation of snow cover, and the percentage

Figure 7.4. Air photo of the upper part of the Längental catchment on June 26, 1989, showing grid elements 25 × 25 m. (By permission of Bundesministerium für Landesverteidigung. From Blöschl et al., 1991b; reproduced with permission.)

denoted by "too early" (negative frequencies in Figure 7.6) refers to elements with bare ground simulated and snow cover observed. For example, on south-facing slopes with slopes around 30° and elevations > 2400 m (i.e. the upper part of the catchment) Figure 7.6 indicates that for 25 % of the pixels in this class, snow cover was simulated but bare ground observed, and for 10 % of the pixels in this class, bare ground was simulated but snow cover observed. The rest of the pixels in this class (i.e. 65 %) were correctly simulated as either snow covered or bare. For most terrain classes, the simulation errors are less than 10 % which indicates good model performance. Figure 7.6 also indicates that there is a certain symmetry about west and east facing slopes, whereas the graph for north- and south-facing slopes is nearly antisymmetric, with a tendency for south-facing

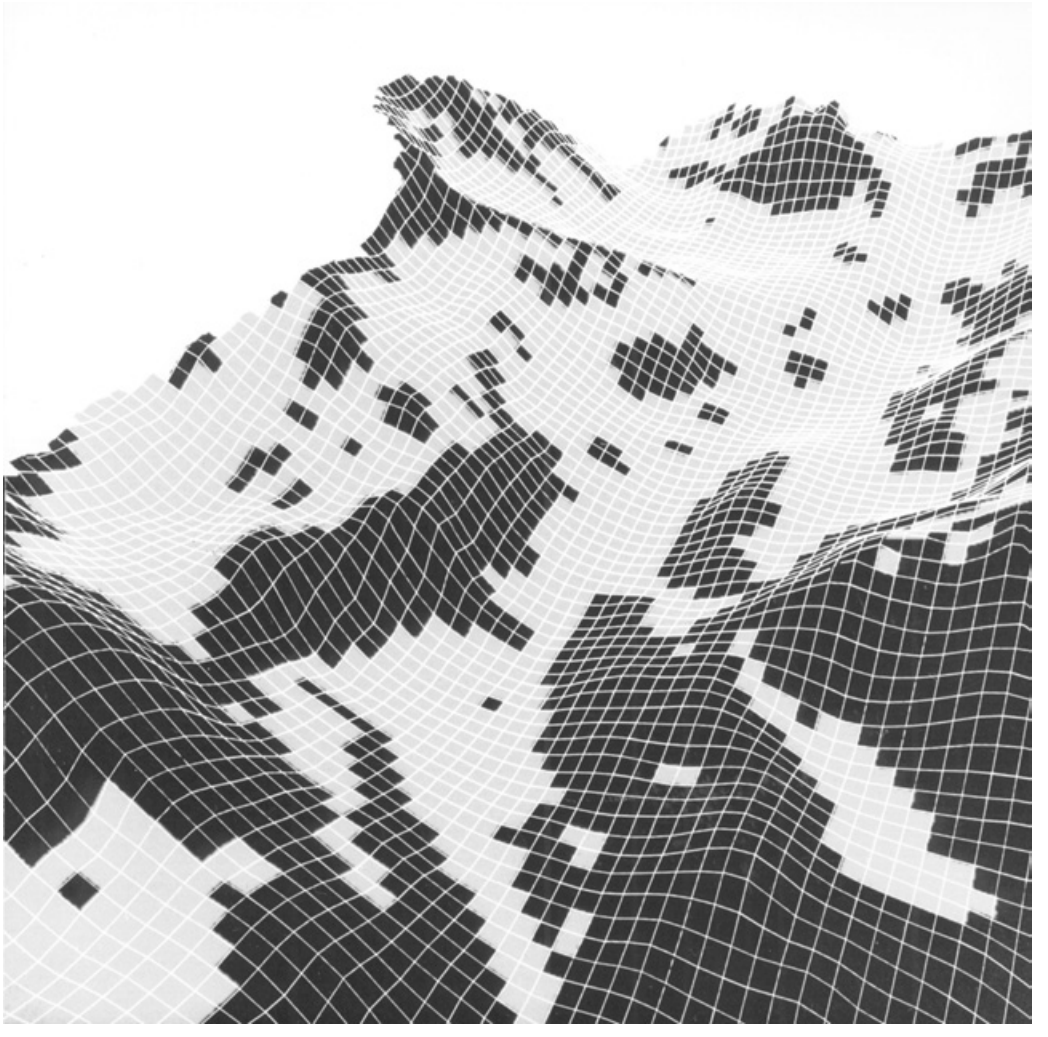

Figure 7.5. Simulated snow cover on June 26, 1989. Dark areas denote bare ground and light areas denote snow cover. (From Blöschl et al., 1991b; reproduced with permission.)

slopes to have too much snow in the model. This tendency suggests that errors are related to solar radiation and specifically to albedo. There are two possible reasons for this. (a) Albedo tends to decrease with the increasing grain size associated with metamorphism (Colbeck, 1988). On south-facing slopes more energy is available for metamorphism and hence albedo will decrease more rapidly with time than on north-facing slopes. This aspect dependence of albedo has not been accounted for in the model. (b) An alternative explanation is a general overestimation of albedo along with an overestimation of sensible and latent heat fluxes or longwave radiation inputs. Although on average over the catchment these two potential errors may compensate, their aspect dependence does not, as there may be too little net solar radiation input on south-facing slopes as compared to north-facing slopes.

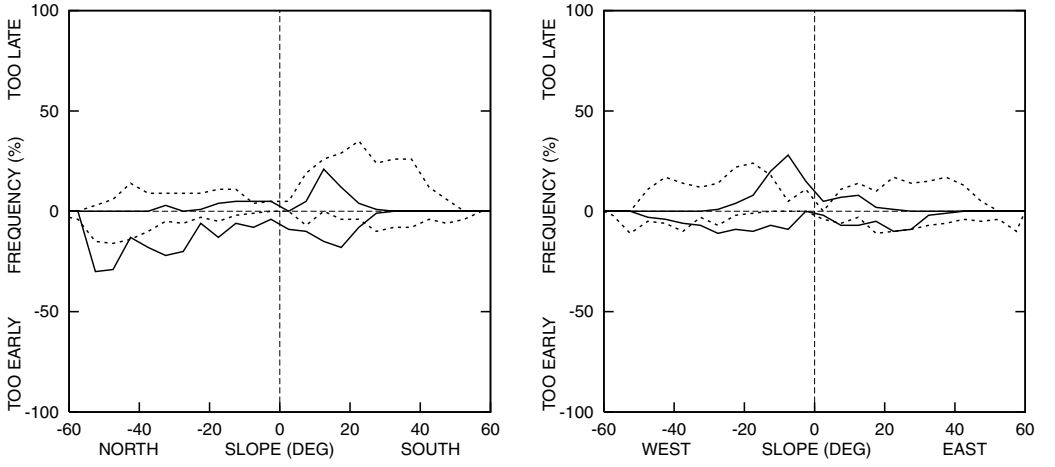

Figure 7.6. Percent errors in snow cover for various slope and aspect classes, June 26, 1989 (too late: snow cover simulated, bare observed; too early: bare simulated, snow cover observed). The dashed lines refer to the upper part of the catchment (above 2400 m) and the solid lines refer to the lower part.

Overall, the comparison of observed and simulated snow cover patterns indicates that the basic model assumptions are realistic. However, there are subtle differences that are very useful in diagnosing model inadequacies. In a parameter sensitivity study (Blöschl et al., 1991a) it was found, not surprisingly, that catchment runoff volume was very sensitive to a parameter controlling the average snow water equivalent in the catchment while it was much less sensitive to the spatial variability of snowmelt due to differential melting. On the other hand, percent error in snow cover (as in Figure 7.6) was highly sensitive to a number of model parameters associated with differential melting including albedo and parameters of equation (7.3). It can therefore be expected that catchment runoff and snow cover patterns are complementary in identifying an appropriate model structure, but the snow cover patterns allow a better identification of individual processes. This complementary information underscores the value of spatial pattern measurements and comparisons in model validation if one is interested in a model of snow cover processes that is close to reality.

7.5 REYNOLDS CREEK CASE STUDY

The Upper Sheep Creek sub-basin within the Reynolds Creek Experimental Watershed has been the location of a detailed study on snowpack variability (Cooley, 1988). Upper Sheep Creek (Figure 7.7) is a 26 ha sub-basin located on the east side of the Reynolds Creek Experimental Watershed (Robins et al., 1965) in the western U.S. rangelands, Idaho. Elevations range from 1840 to 2040 m. The terrain is undulating with maximum slopes of 25°. The vegetation is mostly low sagebrush and mountain sagebrush. Aspen grow in a strip along the north-east facing slope where snow drifts form. Severe winter weather and winds keep the aspen dwarfed to a height of about 4 m. Average annual precipitation is

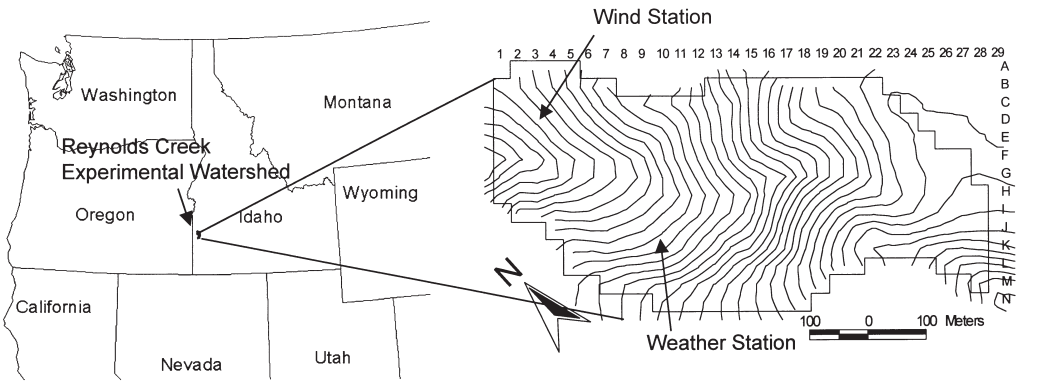

Figure 7.7. Map of Upper Sheep Creek basin within Reynolds Creek Experimental Watershed. Contour interval is 5 m. The catchment outlet of Upper Sheep Creek is on the left.

about 500 mm, with ephemeral runoff usually between February and July when it is generated by snowmelt from deep drifts on the north-east facing slopes. Temperatures average 17 °C in summer and −3 °C in winter (Figure 7.2, solid lines). Various instruments that continuously monitor precipitation, incoming solar radiation, wind direction and speed, air temperature, relative humidity, snowmelt (snowpack outflow) and soil moisture and temperature were operated from 1984 to 1996. In addition, snow depth and snow water equivalent measurements at 30 m grid spacing were obtained on a number of occasions during this interval using standard snow sampling techniques and the Rosen type snow sampler (Jones, 1983). Each snow sample consisted of inserting the snow tube into the snowpack to the soil surface, recording the depth of the snowpack, removing the tube and recording the snow water equivalent as the residual of the weight of the tube and snow sample minus the weight of the empty tube. Manpower limitations were such that it required two storm-free days to fully sample the complete 30 m grid (i.e. about 300 sampling points in space). As a result, typically from four up to nine surveys were done in each year of sampling, attempting to measure the build up and peak snow accumulation followed by ablation. Density was determined for each sample at each grid point by dividing measured snow water equivalent by measured depth. The advantages of this type of snow sampling procedure are the amount of information obtained, i.e. snow depth, snow water equivalent and snow density at each sample point as opposed to more common methods of taking numerous snow depth measurements but only very few snow density samples. When the snow cover exhibits considerable variability in depth as is the case at Reynolds Creek, the density of the snowpack also exhibits considerable variability, and this variability cannot be described by only a few measurements. The disadvantage of this type of sampling procedure is the amount of manpower required to get enough samples to define a pattern. Also, there are snowpack conditions that limit its applicability, such as shallow very dry snow where the snow sample will not stay in the tube and therefore a snow water equivalent cannot be determined, although a depth can still be recorded. Ice lenses in the deeper snowpack can also make it difficult or impos-

sible to collect samples of the snow water equivalent, but depth can usually be obtained by repeated insertions of the snow tube in the same hole until the soil surface is reached.

The patterns of snow accumulation and melt at Upper Sheep Creek are dominated by drifting (Figure 7.8). Snow accumulation usually begins in November and first appears on north-facing slopes and in brushy pockets. As snowfall increases, the upper edges of drifts start to build on the leeward side of the ridges and a general snow cover forms over most of the remaining catchment area. Ridges and south-facing exposures usually experience several periods of snow accumulation and melt during the winter due to strong winds and solar radiation. The general snow cover and drifts normally continue to increase in depth (and width in the case of drifts), often absorbing rain which occurs during occasional warm periods, until maximum accumulation is reached, typically near the beginning of April. After maximum accumulation occurs and melt begins, the ridges and south-facing slopes are generally depleted of snow in a matter of hours. The general snow cover melts next and most of the snow is melted within a few warm days, leaving only the isolated drifts. These drifts persist, sometimes into June or July, sustaining streamflow into late spring and summer.

A typical snow depth distribution is shown in Figure 7.9 for April 4, 1984 which represents conditions near the time of maximum accumulation and shortly after a snowfall event (also see Cooley, 1988). This illustrates the pattern of accumulation as it has been influenced by wind redistribution and variable radiant energy. Depths varied from 0 to 3.8 m. The spatial variations in density for April 4, 1984 are shown in Figure 7.10. Densities on this day were noted to vary from less than 0.15 g/cm^3 to over 0.50 g/cm^3, and appeared to be related mainly to depth, with density larger where the snow is deeper. This figure illustrates the obvious limitations of uniform density assumptions, particularly when wind drift is important.

The model used to simulate the spatial patterns of snow accumulation and melt at Upper Sheep Creek was the Utah Energy Balance (UEB) model which was applied at each 30 m grid point at the same locations as the snow sampling grid. The UEB model is a single layer physically based point energy and mass balance model for snow accumulation and melt (Jackson, 1994; Tarboton et al., 1995; Luce et al., 1997, 1999). The snowpack is characterised using two primary state variables, snow water equivalent, W [m], and the internal energy of the snowpack and top layer of soil, U [kJ m^{-2}]. U is defined as zero when the snowpack is at 0 °C and contains no liquid water. These two state variables are evolved according to energy and mass balance equations accounting for all terms in the energy and mass balance, namely: net solar radiation, incoming longwave radiation, outgoing longwave radiation, heat from precipitation, ground heat flux, sensible heat flux, latent heat flux, heat removed with melt water, precipitation, melt rate and sublimation rate. The model is driven by inputs of precipitation, air temperature, humidity, wind speed and incoming solar radiation. Physically based representations for the energy and mass fluxes are used. Snow surface temperature, a key variable in calculating latent and sensible heat fluxes and

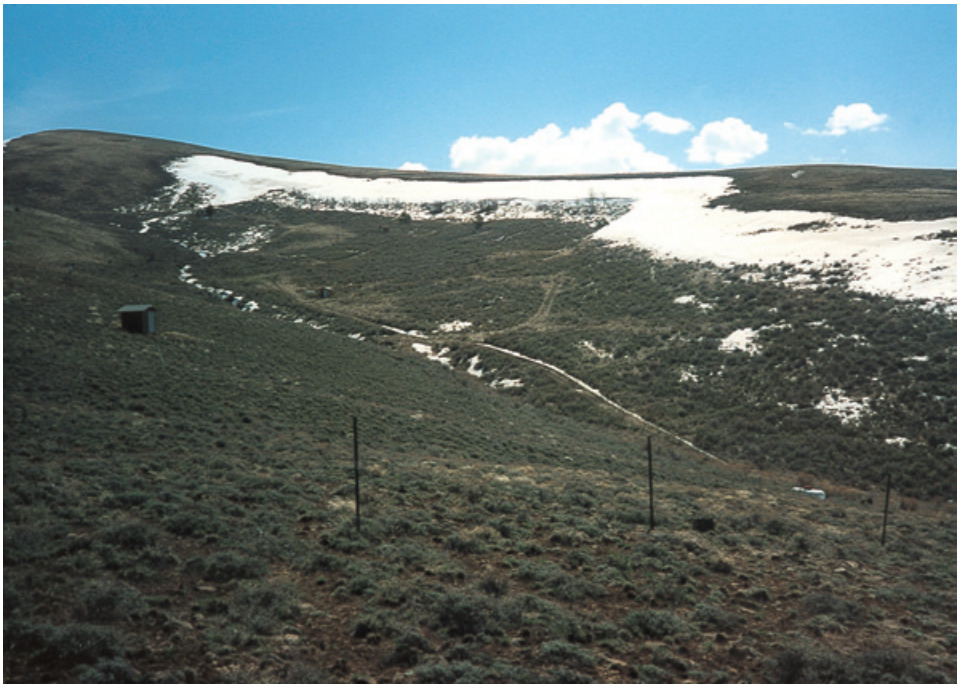

(a)

(b)

Figure 7.8. Photographs of snowdrifts (a) at Upper Sheep Creek; and (b) in Reynolds Creek Experimental Watershed.

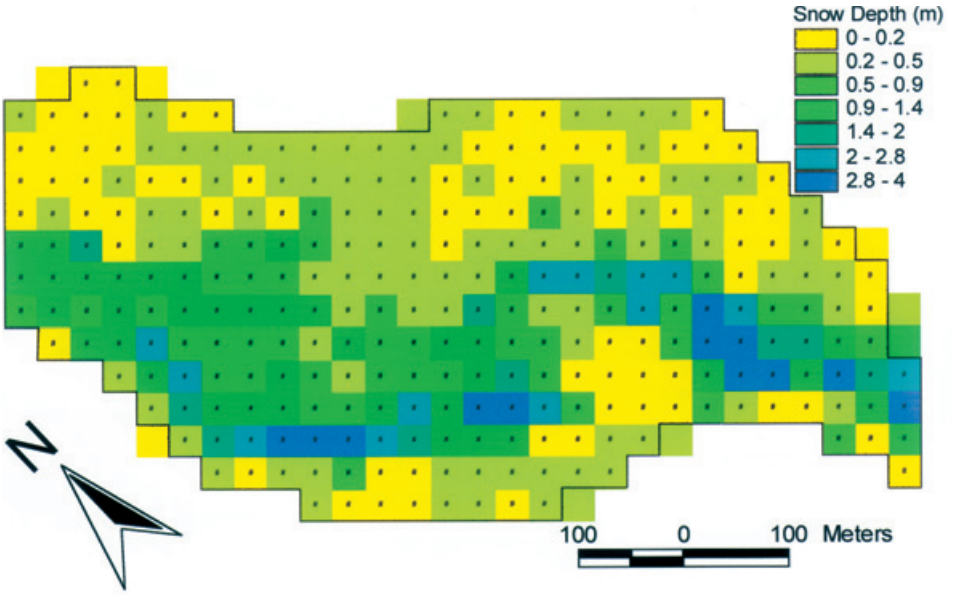

Figure 7.9. Snow depths at Upper Sheep Creek Watershed on April 4, 1984.

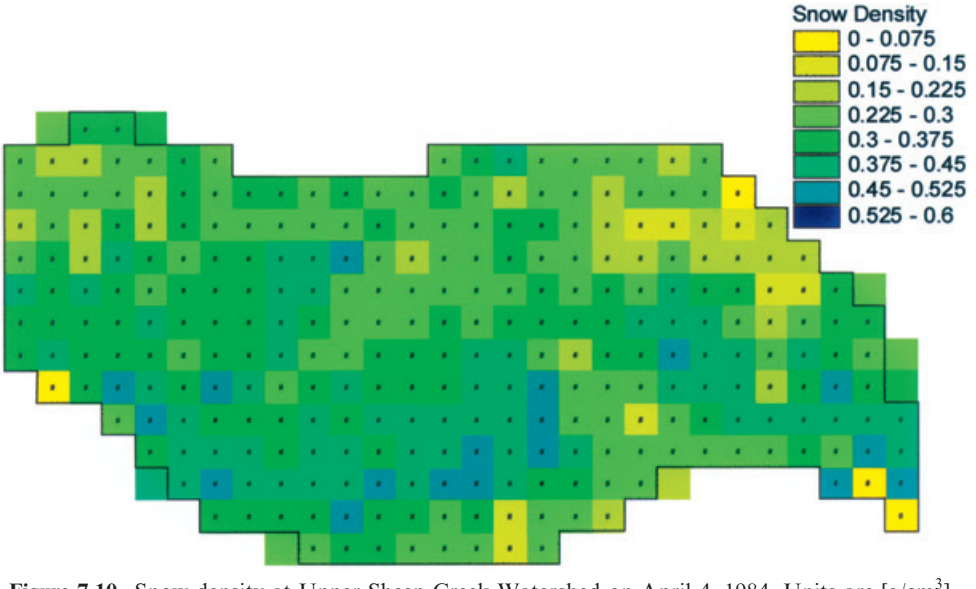

Figure 7.10. Snow density at Upper Sheep Creek Watershed on April 4, 1984. Units are [g/cm^3].

outgoing longwave radiation, is calculated from the energy balance at the surface of the snowpack where incoming and outgoing fluxes must match. This allows the snow surface skin temperature to be different from the average temperature of the snowpack as reflected by the energy content. This reflects the insulating effect of snow and facilitates good modelling of the surface energy balance without needing to introduce multiple layers and detail of within-snow energy transfers. The model was run on a six-hourly time step.

Inputs of precipitation, temperature, relative humidity and incoming radiation were measured at a weather station located centrally within the catchment (Figure 7.7). This location is sheltered and below the drift, so it is subject to minimal wind deposition and transport effects. Wind speed was measured at a more exposed location (Figure 7.7) in order to be more representative of general wind flow. With the exception of solar radiation, the climate variables were assumed to be spatially uniform. Distributed solar radiation was calculated in two steps. Pyranometer (incoming solar radiation) data at the weather station was used to calculate an effective atmospheric transmission factor. Local horizons, slope and azimuth were used to find local sunrise and sunset times and integrate solar radiation received on the slope for each time step. The calculated atmospheric transmission factor characterised cloudiness for incoming longwave radiation calculations.

The UEB model does not represent the physics of snow drifting. Since observations show this to be important at Upper Sheep Creek, we accommodated this in the modelling through the use of a snow drift factor (Jackson, 1994; Tarboton et al., 1995). The fraction of precipitation (measured at a gauge) falling as rain or snow is modelled as a function of temperature. The fraction falling as snow is assumed to be susceptible to drifting. Snow accumulates in some areas (mainly the lee of ridges) and is scoured from other areas (mainly ridges and windward slopes). In the model this redistribution process, which really occurs after snowfall, is lumped together in time with the occurrence of snowfall. Snow accumulation in a grid is modelled as snowfall multiplied by a drift factor, F, which is a spatial field of distinct factors for each grid location. F does not change in time. F is greater than 1 where accumulation is enhanced by drifting and less than 1 where scour occurs. In the application to Upper Sheep Creek, F was estimated by calibrating the snow water equivalent obtained from the snow model at each cell, W_m, against the observed values, W_o. The discrepancy between observations and predictions over an interval between measurements is attributed to drifting and F is adjusted until W_m equals W_o at the end of the interval. The calibration of F assumes that the snowmelt model correctly accounts for all other processes (melt, sublimation, condensation, etc.) affecting the accumulation and ablation of snow water equivalent. Figure 7.11 gives drift factors F calibrated to match the snow water equivalent on February 25 and March 26, 1986 (Jackson, 1994; Luce et al., 1998). Values of F ranged from 0.2 to 6.8 with an average of 0.975.

The UEB model was used with drift factors calibrated from February–March 1986 to predict snow-cover patterns and surface water inputs for the 1993 water year. This is a genuine split sample test (see Chapters 3 and 13), as the calibration

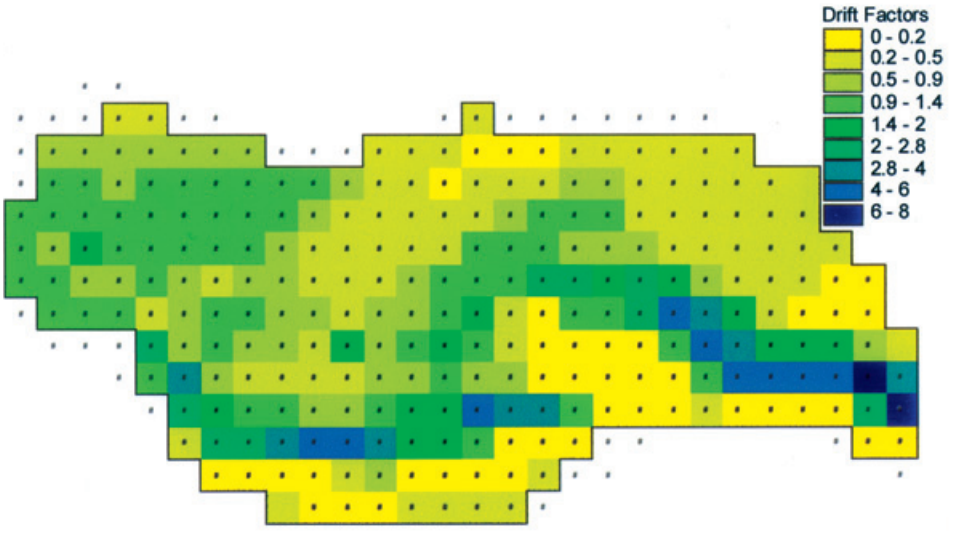

Figure 7.11. Upper Sheep Creek drift factors calibrated from the 1986 snow cover period. (After Jackson, 1994.)

and verification periods do not overlap. The results comprising maps of observed and simulated snow water equivalent over Upper Sheep Creek are shown in Figure 7.12a and b, respectively. From a visual comparison, the observed and simulated patterns are quite similar but there are a few subtle differences. First, the simulated drift is more sharply defined than the observed drift, and snow water equivalent is overestimated in the north-west of the catchment. This suggests that there was less snow drift in 1993 than in 1986. One potential remedy would be to use a deterministic wind drift model (e.g. Liston and Sturm, 1998) to better represent the variability of drifting from year to year. This is an option we are pursuing in current research. Another difference between observed and simulated patterns is that the model has a tendency to melt snow too rapidly, as evidenced by the disappearance from the model of general snow cover on and around pixel J10 (Figure 7.7) in early April. In the observations this snow cover persists about two weeks longer. This rapid melting tendency is also noted in Table 7.1, where during the ablation period simulated basin average totals are less than observed. Plotting observed against simulated grid snow water equivalent for each date (Figure 7.13) shows that the model generally overestimates snow water equivalent for locations with moderate to high snow water equivalents, but underestimates snow water equivalent where there is little snow, with systematic overestimation most apparent in the early melt season. This is consistent with the interpretation of a more uniform snow pattern in 1993 than in 1986, made above.

A sensitivity study was performed in order to assess the relative importance of the various sources of spatial snow variability (Luce et al., 1997, 1998). Results from one of the scenarios are shown in Figure 7.12c and Table 7.1 where the model was run without the effect of drifting, i.e. the drift factor was set to 1 everywhere. In this scenario, spatial variability in snow water equivalent is

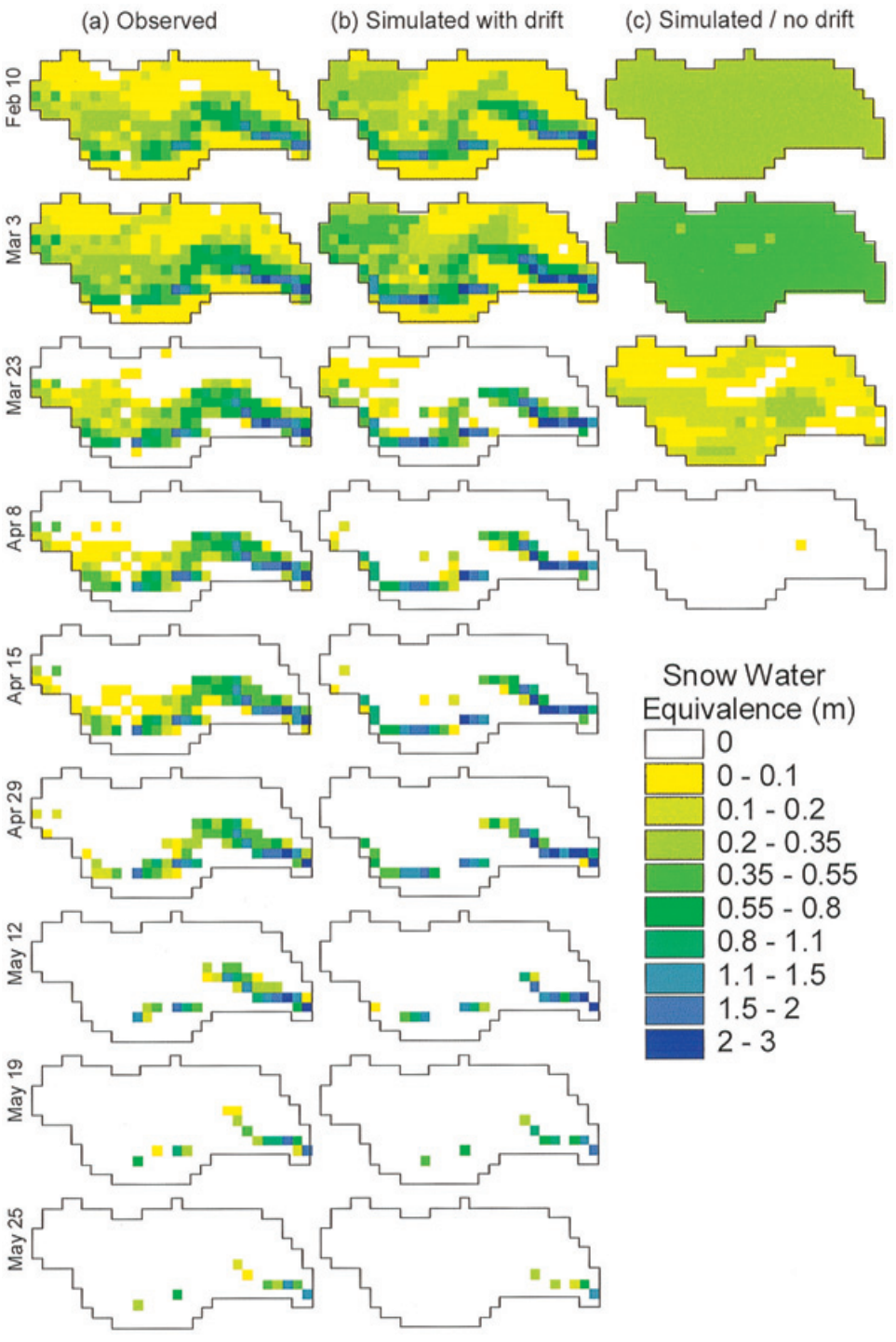

Figure 7.12. Snow water equivalent over Upper Sheep Creek on 9 dates of snow survey in 1993 for: (a) observed; (b) simulated with drift; and (c) simulated without drift. (From Luce et al., 1998. Copyright John Wiley and Sons Ltd. Reproduced with permission.)

Table 7.1. Basin-averaged snow water equivalent (m) from observations and models

Date	Observed	Model with drift	Model no drift
Feb 10, 1993	0.22	0.28	0.28
Mar 3, 1993	0.28	0.38	0.39
Mar 23, 1993	0.23	0.23	0.10
Apr 8, 1993	0.18	0.16	0.00
Apr 15, 1993	0.17	0.16	0.00
Apr 29, 1993	0.13	0.13	0.00
May 12, 1993	0.09	0.07	0.00
May 19, 1993	0.04	0.03	0.00
May 25, 1993	0.02	0.01	0.00

mainly due to topographically induced variation of radiation inputs. Figure 7.12c shows that in the no-drift case the spatial variability in snow water equivalent is much smaller than in the original case where snowdrift is included. This smaller variability highlights that, at Upper Sheep Creek, variation due to wind drift is vastly more important than any other source of variation including radiation. For a model to approach reality it is essential to properly represent wind drift processes. The other difference between the no-drift case and the original case with snowdrift is that in the no-drift case, the snow cover disappears much earlier, and the average basin snow water equivalent is significantly lower (Table 7.1). This bias is clearly due to the nonlinear nature of snowmelt processes, where the spatial average of spatially distributed simulations may be very different from simulations based on spatial averages (Blöschl, 1999). This sheds some light on the limitations of the use of effective parameters. In environments where the snow cover is as heterogeneous as in this case study, effective parameter values of snow models are likely to be greatly in error. More extensive sensitivity analyses (Luce et al., 1997, 1998) including comparisons with single or two-region models, corroborate these findings and show that the fully distributed model with distributed drift multiplier is the only model (of the ones tried) that predicts significant melt late in the season, coinciding with the observed rise of the streamflow hydrograph.

This underscores the value of a spatially distributed modelling approach incorporating spatial patterns describing the variability of the drift multiplier. The essential prerequisite for this type of modelling is the availability of spatial data, such as the observed patterns of snow water equivalent at Upper Sheep Creek. For applying this modelling approach to larger catchments, methods will be needed for predicting drift factors or alternative methods for representing small scale variability.

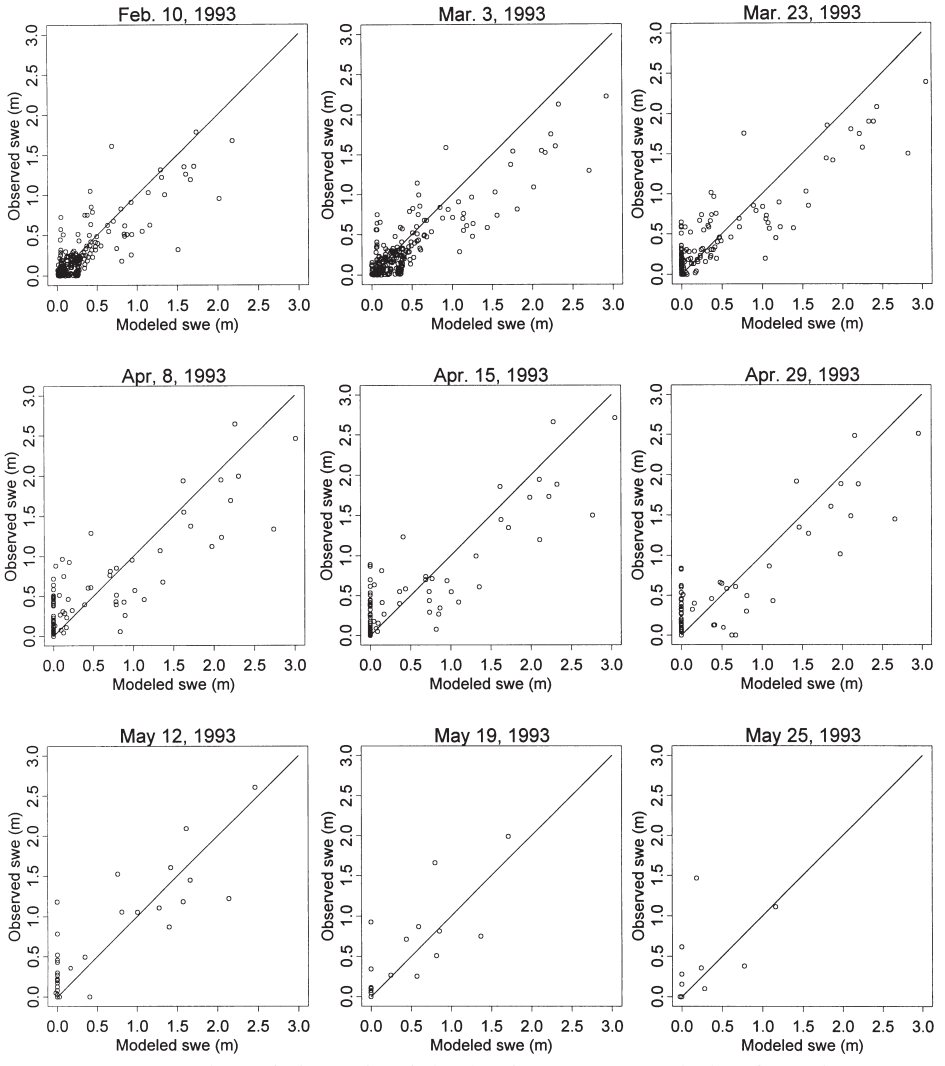

Figure 7.13. Comparison of observed and simulated snow water equivalent for each snow survey date. Each point represents one grid value within the catchment. (From Luce et al., 1998. Copyright John Wiley and Sons Ltd. Reproduced with permission.)

7.6 CONCLUSIONS

This chapter has examined the processes that lead to spatial variability in snow accumulation and snowmelt in the context of two case studies. Although the settings and methods of the two case studies were very different, the basic strategy of model evaluation was similar and consisted of process-based reasoning and analysis of both visual comparisons and pointwise statistical comparison of simulated and observed patterns. In both case studies, observed spatial patterns could be simulated only when particular processes were represented spatially.

At Kühtai the general snow patterns could be well represented by the spatial variability of radiation and a statistical representation of snow drifting but some aspects of the measured patterns could not be simulated. These aspects included enhanced snowmelt in cirques due to longwave emission from surrounding terrain, which was diagnosed from an overprediction of snow cover in the cirques; formation of a snow deposit at the base of a cliff due to avalanching which was diagnosed from an underprediction of snow at the base of the cliff; significant small-scale spatial variability of snow which was diagnosed from a visual comparison of patterns; and enhanced metamorphism and hence more rapid decrease of albedo on south-facing slopes as compared to north-facing slopes which was diagnosed from a slight tendency for overestimating snow on south-facing slopes. For improved simulations of the spatial variations of snow accumulation and melt these processes need to be modelled explicitly.

At Reynolds Creek the general snow patterns could be represented well by the spatial variability of snow drifting. However some aspects of the measured patterns could not be simulated. These included a slightly more uniform snow distribution due to less redistribution of snow in the later year relative to the earlier year. This discrepancy was diagnosed from a visual comparison of patterns as well as from a slight overestimation of snow water equivalent for locations with moderate to high snow water equivalents but a slight underestimation of snow water equivalent for locations with below average snow water equivalents as indicated by error statistics. This indicates that the drift factors computed from the 1986 snow data were more variable than the actual drift in 1993. More generally speaking, this means that the model calibrated on one data set does not necessarily perform as well on an independent data set. At Reynolds Creek the dominance of wind drift was illustrated by running a model which ignored drift but incorporated spatial variability in other processes. This resulted in an almost uniform pattern.

Both case studies have demonstrated the value of observed spatial patterns for diagnosing the performance of individual model components and for identifying model structural issues and parameterisation. It is clear that the patterns have provided more insight than a few point data or catchment average values from runoff would have provided. We believe that, in the future, comparisons of distributed model output with observed snow patterns will become part and parcel of any snow-modelling exercise.

ACKNOWLEDGEMENTS

The work of the first author on this was supported by the U.S. Environmental Protection Agency (agreement no: R824784) under the National Science Foundation/Environmental Protection Agency Water and Watersheds program. The second author wishes to thank the Fonds zur Förderung der Wissenschaftlichen Forschung, Vienna, project nos. P6387P, P7002PHY, and J0699-PHY for financial support.